INFLUENCE OF THE FILLING MATERIAL PROPERTIES ON PRESSURE IN HBC FUSE. COMPARISON BETWEEN EXPERIMENTAL RESULTS AND SIMULATION

Bussière William[1], Rochette David[2] and Pellet René[3]

LAEPT CNRS UMR 6069 [1], Phys. Bât. 5 – 24, Av. des Landais – F63177 AUBIERE CEDEX FRANCE, william.BUSSIERE@laept.univ-bpclermont.fr
LAEPT CNRS UMR 6069 [2,3], Phys. Bât. 5 – 24, Av. des Landais – F63177 AUBIERE CEDEX FRANCE, david.ROCHETTE@laept.univ-bpclermont.fr [2], rene.PELLET@laept.univ-bpclermont.fr [3]

Abstract: By varying the mean granulometry and the packing density of the arc quenching material (silica sand), we show the influence of the silica sand morphometric properties on the pressure evolution during the HBC fuse working. Pressure measurements are made using piezoelectric transducers inserted at various lengths taken from the fuse strip plane. The measurements are compared with the results get from the simulation of the energy withdraw within a granular material. Both types of results show that the pressure evolution is strongly correlated with the electric power evolution and the morphometric properties.

Keywords: H.B.C. fuse, pressure, packing density, mean granulometry, porosity, Darcy's law and Forchheimer's law.

1. Introduction

High Breaking Capacity (H.B.C.) fuses are classically made of four main elements: an insulating cartridge, two metal electrodes, a fuse strip (silver), and the arc quenching material, granular silica sand in our case. The morphometric properties of the silica sand, namely the mean granulometry, the packing density, the form factor, play an important role during the prearcing and arcing times, depending on the fault current value.

Silica sand is widely used in H.B.C. fuses [1-2] because of its ability to withdraw the energy brought by the fault current from the arc column. To quantify more precisely the influence of the silica sand properties, we give experimental and simulated results concerning three main points.

- The dependence between the mean granulometry and the maximum packing density.
- The influence of the these two properties on the electrical parameters and pressure evolution.
- The correlation with the mechanical forces.

In Section 2. we give the experimental results concerning the morphometric properties and the pressure measurements. In Section 3. we give the results obtained with the simulation. The results are discussed in Section 4.

2. Experiment

2.1. Experimental device

The fuse used in the tests is designed so as to reproduce the breaking phenomenon as in an industrial fuse. The main discrepancy is that the energy is delivered by means of a capacitor bank discharge (C = 16.5 mF, L = 145 µH, R = 270 mΩ). The shape of the current waveform is due to the (R,L,C) value of the capacitor bank. The prearcing plus arcing time is about 4 ms. The prearcing time is about 0.85 ms. The maximum of the electric power is observed in the time interval from ~ 1.7 ms to ~ 2.2 ms.
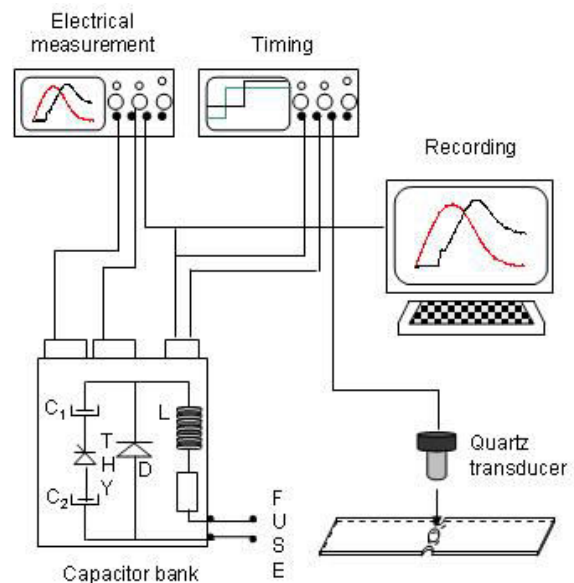

Fig. 1: Schematic diagram of the test set-up. The pressure sensor is directly above one of the fuse element constriction.

To measure the pressure, we have designed a specific set-up taking into consideration the fulgurite growth, especially at right angles to the fuse strip

notches. The cartridge is made of Polyoxymethylene and is chosen cylindrical. The beginning of the discharge ($di/dt > 0$) is set as the zero value for the time scale.

Two TEK TDS 224 oscilloscopes are used do display the current through and the voltage across the fuse, and the pressure inside the granular filler. The pressure is measured using a piezoelectric pressure transducer whose frequency response is 150 kHz (Kistler quartz high pressure sensor 601A).

2.2. Silica sand

The silica sand used in the tests is the same as the industrial one. It is high purity quartz sand (99.80 %) whose mean granulometry and packing density are checked carefully in each experiment.

Table 1. Characterization of the silica sand. Each of the granulometric intervals is 50 μm wide. Each of the packing density letter represents 0.04 g.cm^{-3}.

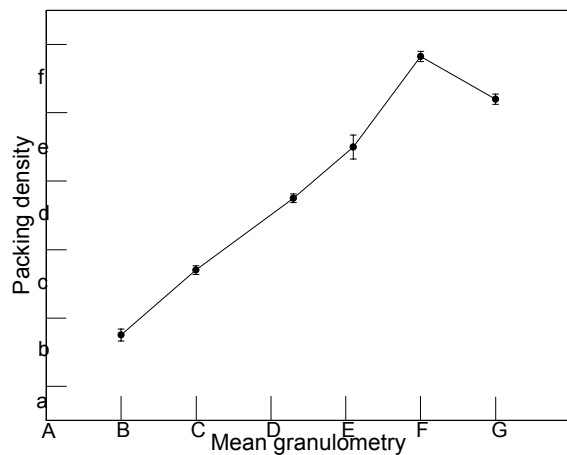| Parameter	Value
Real density (g.cm^{-3})	2.65
Apparent density (g.cm^{-3})	1.50
Granulometry (μm)	A, B, C, D, E, F, G
Packing density (g.cm^{-3})	a, b, c, d, e, f

Fig. 2: Packing density of the silica sand versus the mean granulometry. The upper limit of the mean granulometry is inferior to 1000 μm. The upper limit of the packing density is inferior to 2 g.cm^{-3}.

For each mean granulometry in Fig. 3, we give the highest packing density value which we obtain using a specific mechanical device. The error bars represent the statistical deviations around this highest mean value calculated using at least five experiments. For the mean granulometric interval studied (A .. G), the packing density varies linearly with the mean granulometry, excepted for the interval symbolyzed G for which we obtain a reproducible value.

2.3. Fulgurite

Many publications have pointed out the role of the arc quenching material on the breaking phenomenon in a fuse [1-2]. A direct observation using fast imagery clearly shows the spreading of the fluid from the centre of the arc channel towards the surroundings [3].

Due to the fusion and the vaporization of the fuse element and the very near layer of silica sand, the pressure inside the arc channel gradually increases, at the condition that the energy brought by the fault current is sufficient enough. This implies the increase of the fulgurite thickness (Fig. 4).

Thus, as a first approximation, we can suppose that the fulgurite thickness is both the result of the maximum pressure and the fluid spreading in the interstices of the granular fuse filler.
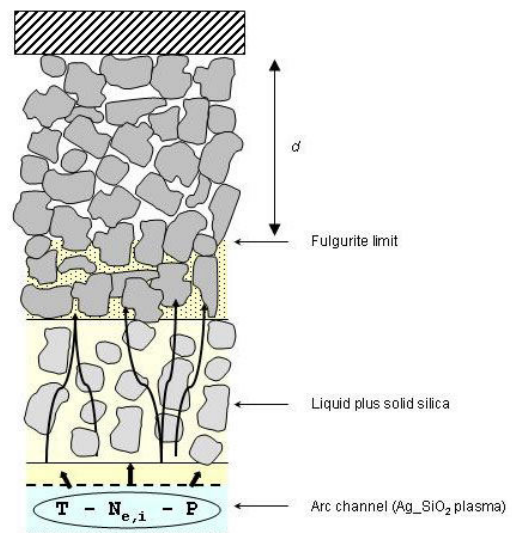

Fig. 3: Various locations of the pressure transducer (*d*) defined taking into consideration the growth of the fulgurite thickness.

Moreover, to avoid a direct contact between the pressure sensor and the hot surroundings of the fulgurite, we have used the results concerning the evolution of the fulgurite thickness versus the mean granulometry [4]. From these results, we can roughly estimate the minimum length *d* for the pressure measurement for each mean granulometry.

2.4. Pressure measurement

All the tests have been performed with the same configuration given in Table 2. The short circuit current is about 3.2 kA; the di/dt is about 2.1×10^6 A.s^{-1}.
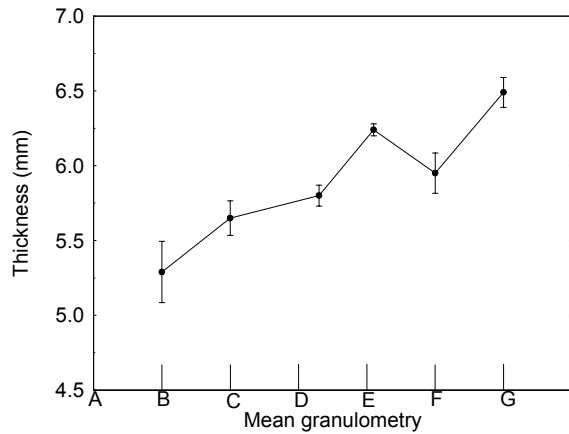
Fig. 4: Evolution of the thickness of the fulgurite versus the mean granulometry.

Table 2. Configuration of the tests. U, stored voltage ; E, total dissipated energy ; I².t, total value of $\int i^2(t)\,dt$; $t_{PREARCING}$, prearcing time ; t_{TOTAL}, prearcing plus arcing time ; d, length between the pressure sensor and the fuse strip.

Parameter	Value
U (V)	460
E (J)	~ 1100
I².t (A².s)	~ 7000 to 9000
$t_{PREARCING}$ (ms)	~ 0.85
t_{TOTAL} (ms)	4.00
d (mm)	7 – 9.5 – 12 – 17
Mean granulometry	B – D – F

For each value of *d* (Fig. 3), at least three experiments were done with the same morphometric conditions (mean granulometry and packing density). A typical set of electrical measurements is given in Fig. 5 in the case of a 460 V- stored voltage. The prospective fault current is about 3.2 kA. The pressure evolution is showed in Fig. 6.

We do not attempt to measure the pressure inside the arc channel by means of the quartz pressure sensor. In fact, the sensor should be damaged due to the very high temperature of the fuse plasma. Thus we measure the pressure of the sand grains on the sensor. This mechanical strength is directly due to the pressure propagation from the plasma to the surroundings, successively through the liquid layer immediately after the plasma, the fused plus solid silica layer, and then the solid sand grains.

The pressure evolution can be divided in three intervals.

- At the beginning of the arcing time: the over pressure due to the arc ignition is the result of the fusion and vaporization of the silver fuse strip. The pressure increase is clearly observed for the smaller *d* values.
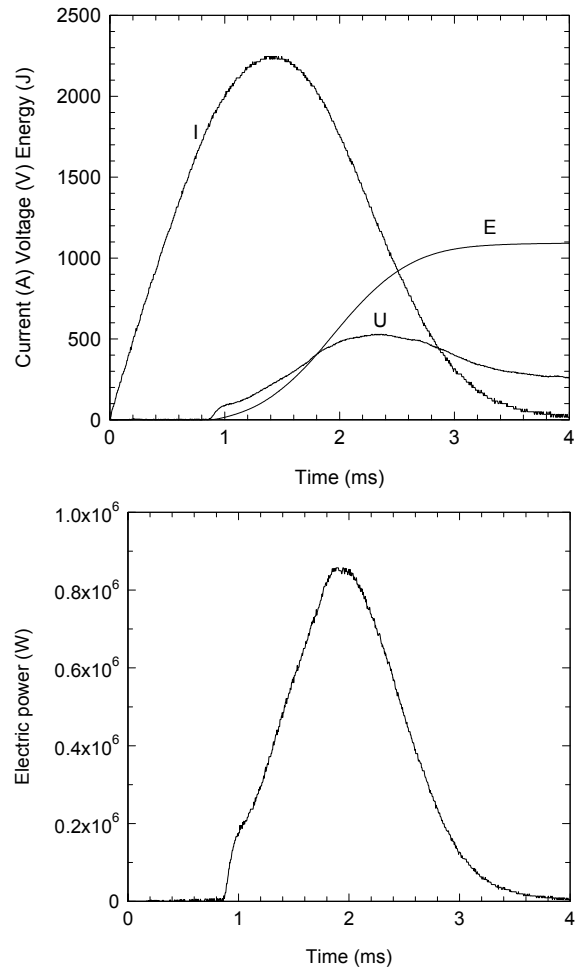

Fig. 5: Evolution of the electric current through and the voltage across the fuse, the total dissipated energy, and the electric power.

- Once the plasma is initiated, the fuse strip and the very near sand grains are gradually melted and vaporized. Thus the pressure increases continuously until the maximum pressure.
- Once the maximum pressure is obtained, the pressure decreases down to values around the atmospheric pressure. This pressure decrease is linked to the dissipated energy rate which is due to the capacitor bank characteristics.

The observed values are inferior to $17\,10^5$ Pa whatever the test configuration. These values are clearly less than those measured in [5]: $50\,10^5$ Pa for the maximum. We can suppose that the discrepancy is due to the fact that we measure the mechanical strength due to the sand grains, whereas in [5], the measured pressure is the result of the shock wave due to the plasma pressure transmitted to the sensor. Thus we can approximate that the maximum true value is in the interval $[17-50]\,10^5$ Pa.
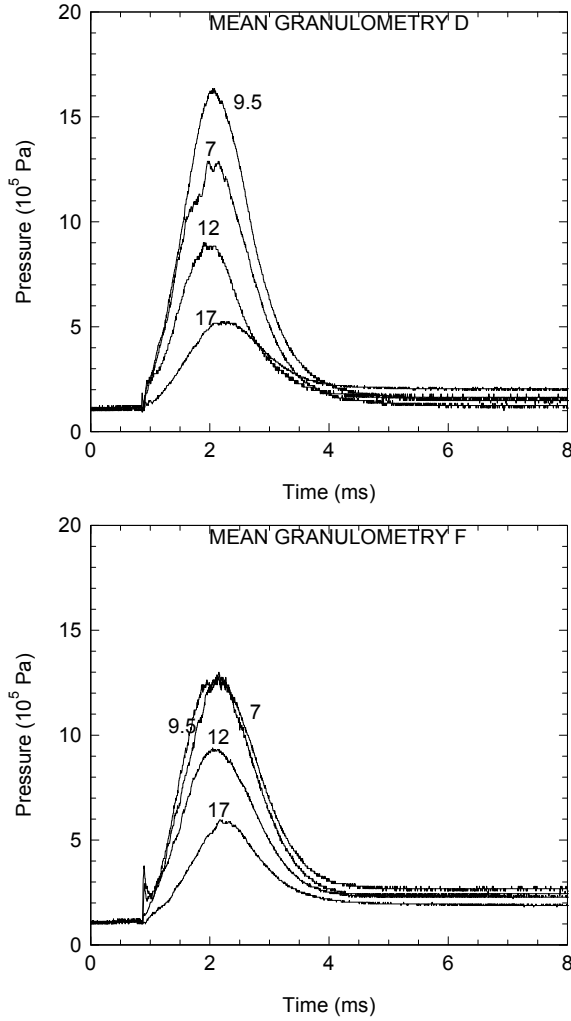
Fig. 6: Evolution of the absolute pressure versus time for the three mean granulometries symbolized B, D, F. The numbers represent the length d in mm.

3. Modeling

We present an one-dimensional model to describe the fluid flow and the heat transfer in HBC fuse. The model is based on the compressible Euler equations for perfect gas coupled with a porous media model taking into account the mechanical interaction between the fluid and the silica sand and the heat transfer between hot fluid and cold silica sand [6-7]. In addition to describe the solid temperature evolution, we introduce the heat equation for the solid in porous media [8]. The governing equations are discretized following a finite volume scheme coupled with a fractional step technique and the fluxes are evaluated using the Roe solver [9].

3.1. Mathematical model

The one-dimensional governing equations for single-phase fluid flow in an isotropic, homogeneous porous medium based on the Darcy-Forchheimer model [8] can be written in the following form:

$$\frac{\partial(\rho_f \phi)}{\partial t} + \frac{\partial(\rho_f \phi u)}{\partial x} = r \tag{1}$$

$$\frac{\partial(\rho_f \phi u)}{\partial t} + \frac{\partial(\rho_f \phi u^2 + \phi p)}{\partial x} = p\frac{\partial \phi}{\partial x} - \phi^2 \frac{\mu}{k} u - \phi^3 \beta \rho_f |u|u \tag{2}$$

$$\frac{\partial(E\phi)}{\partial t} + \frac{\partial[(E+p)\phi u]}{\partial x} = pu\frac{\partial \phi}{\partial x} + S - h_{sf} A_0 (T_f - T_s) \tag{3}$$

The physical parameters are ρ_f the fluid density, u the interstitial velocity, p the pressure, E the total energy, T_f, T_s the fluid and solid temperature and ϕ the porosity.

In Eq.(1), the quantity r represents the material source due to the vaporization of the material. In Eq.(2), the expression $\phi^2 \frac{\mu}{k} u$ represents the viscous friction between fluid and grains silica sand where μ is the dynamic viscosity, k is the medium permeability and the term $\phi^3 \beta \rho_f |u|u$ is the Forchheimer flow resistance where β is the Forchheimer coefficient. In Eq.(3), S represents the electrical energy injected in the fuse (Fig.5) and the quantity $h_{sf} A_0 (T_f - T_s)$ is the thermal dispersion representing heat exchanges between fluid and silica sand.

In addition to close the system, we use the ideal gas equation of state:

$$p = (\gamma - 1)\rho_f e \quad \text{with } \gamma > 1,$$

where γ is the ratio of specific heat and e is the specific internal energy.

To model the heat transfer processes with a thermal non-equilibrium between the fluid and solid phases, we introduce the classical heat equation with longitudinal thermal conduction in the solid phase to evaluate the solid temperature T_s:

$$\rho_s c_{vs} \frac{\partial T_s}{\partial t} - \frac{k_{eff}}{(1-\phi)} \frac{\partial^2 T_s}{\partial x^2} = \frac{h_{sf} A_0}{(1-\phi)} (T_f - T_s) \tag{4}$$

where ρ_s denotes the solid density, c_{vs} is the solid specific heat and k_{eff} is the porous media conductivity.

3.2. Source terms

An excess current generates heat at the silver fuse element constrictions and leads to the fusion and vaporization of the silver at the beginning, and vaporization of the silica sand later. In a first approximation, we assume that the rate of vaporized mass is proportional to the electrical power injected in the fuse. The mass source term is given by:

$$r = \delta \frac{S}{H_{vap}}$$

where $\delta \in [0,1]$ represents the percentage of electrical power responsible for silica vaporization. The value of δ is chosen in order to obtain a coherent fluid temperature with the experimental value.

The energy source term has contributions from electrical power and thermal dissipation. The injected energy is characterized by a power density function representing the energy quantity per unit volume and time based on Fig.5.

An great part of the energy injected in the fuse is dissipated by transfer between the hot fluid and the cold silica sand. Following [10] the modelling of the heat transfer is given by:

$$Q = h_{sf} A_0 \left(T_f - T_s \right)$$

where A_0 is the specific surface area and h_{sf} represents the interfacial convection heat transfer coefficient which depends on the fluid nature, the fluid flow regime, the morphology and roughly of silica sand grains.

3.3. Numerical method

In order to obtain an approximate solution of the gas flow model in porous media, we use a fractional step technique [9]: on the one hand we solve separately during a small time step Δt the homogeneous conservative system, and on the other hand the right-hand side terms. Let ρ^n be an approximation of $\rho(t^n)$ at time t^n. In order to obtain an approximation of $\rho(t^{n+1})$ at time $t^{n+1} = t^n + \Delta t$, we first determine an approximate solution of the homogeneous problem using the finite volume scheme of the form:

$$\tilde{\rho}_i^{n+1} = \rho_i^n - \frac{\Delta t}{\Delta x} \left(F_{i+1/2}^n - F_{i-1/2}^n \right)$$

where $F_{i+1/2}^n$ and $F_{i-1/2}^n$ represent respectively the numerical fluxes calculated at the interface cells $x = x_{i+1/2}$ and $x = x_{i-1/2}$ using Roe method. Assumed now that $\tilde{\rho}^{n+1}$ is the approximated solution value at $t = t^{n+1}$ of the previous homogeneous problem, we solve the ordinary differential equation. Numerically, we add the right hand side contribution using a fourth-order explicite Runge-Kutta method.

To compute the solid temperature T_s we use an explicit finite volume method given by:

$$\rho_s c_{vs} T_{i,s}^{n+1} = \rho_s c_{vs} T_{i,s}^n + \frac{\Delta t}{\Delta x} \left(G_{i+1/2}^n - G_{i-1/2}^n \right) - \Delta t \frac{h_{i,sf}^n A_0}{1-\phi} \left(T_{i,s}^n - T_{i,g}^n \right)$$

where central differences are used to determine the fluxes $G_{i+1/2}^n$ and $G_{i+1/2}^n$.

3.4. Numerical results

We present a simulation of an electrical arc discharge through the porous medium using realistic physical parameters. To compare with the measurements, we use the three silica sand granulometries symbolized B, D, F. In steady state, we have determined experimentally the friction coefficients used in the mechanical interaction laws for each granulometry (Table 3).

Table 3. Configuration of the tests. k permeability; β Forchheimer coefficient.

Granulometry	k (m^2)	β (m^{-1})
B	9.3×10^{-12}	1.54×10^5
D	1.5×10^{-11}	1.35×10^5
F	2.6×10^{-11}	1.2×10^5

Computations have been performed using the C++ finite volume library OFELI [11] on a 200 elements mesh composed of two uniform meshes where 100 cells correspond to the first area $x \in [0,2]mm$ and 100 cells to the second area $x \in [2,20]mm$. At the initial time, the system is at rest, the fluid present in the silica sand interstices is at atmospheric pressure and ambient temperature.

We present the plasma pressure evolution during the fuse operation for the three granulometries in Fig. 7. The pressure increases up gradually to the maximum value which falls nearly on the same time of the maximum electric power. The maximum pressure is higher for the smallest granulometry B. The maximum pressure values are in the range from $\sim 19 \ 10^5$ Pa to $\sim 24 \ 10^5$ Pa. At the decrease of the electric power, the pressure decreases. The atmospheric pressure is obtained a little less than ~ 10 ms after the start of the current waveform. The results of the simulation confirm the experiments in so far as: first, a small granulometry implies a more efficient overpressure linked to the voltage increase due to the fuse ; second, considering only the mechanical point of view, the results show that the pressure wave propagation is directly influenced by the grain size and the interstices volume.

The pressure wave propagation in the silica sand during the fuse operation is given in Fig. 8 for the three granulometries.

- Whatever the position in the fuse domain, the pressure increases with decreasing granulometry. The values in Table 4. are consistent with the measurements.
- The comparison of the experiment with the simulation shows that the maximum values are different. This can be due to: first, the pressure wave propagation can imply the rearrangement of the sand grains, and consequently, the

measurement is more or less reproducible ; second, neither the condensation of the vapours in the surroundings of the plasma and the thermal flow in the sand grains are considered in this modeling: the pressure at the surroundings is thus overestimated.
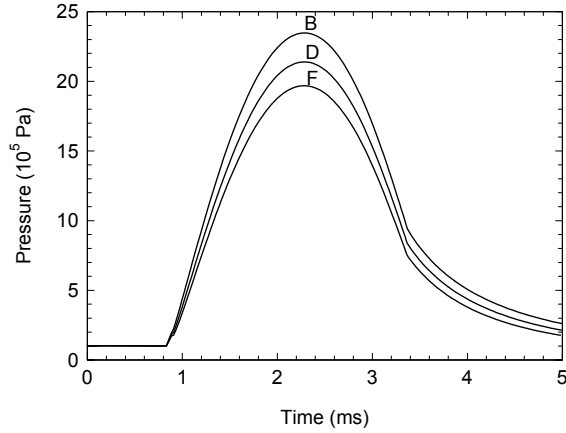

Fig. 7: Evolution of the plasma pressure versus time for three mean granulometry values symbolized B, D, F.

To compare the experimental and simulated evolutions, we give the evolution of the normalized pressure versus time for the granulometry B in Fig. 9. For each type of results, the normalization is realized by dividing the curves by the maximum pressure observed for $d = 7$ mm. The evolutions are similar for $d = 7$ mm and $d = 9.5$ mm. For higher values of d, we observe a significant discrepancy mainly due to two main reasons. First, the modeling restrictions. Second, the observed pressure is obtained for a given d ; due to the presence of the sand grains, the measurement is not unidirectional ; thus, the pressure waveforms responsible for the mechanical strength on the sensor come from different areas in the filler ; this can lead to an overestimation, especially for $d =$ 12 mm and $d = 17$ mm.

The Fig. 10 represents the velocity and the friction forces evaluated at the plasma periphery for the three mean granulometries. The velocities are higher for the biggest granulometry which is consistent with the simulated and experimental pressures. For the small granulometry, the interstices volume is reduced compared to the upper granulometries. Moreover, for the velocity range calculated, we remark that the Forchheimer term is prominent. The Darcy term is clearly less and nearly constant during the arcing time.
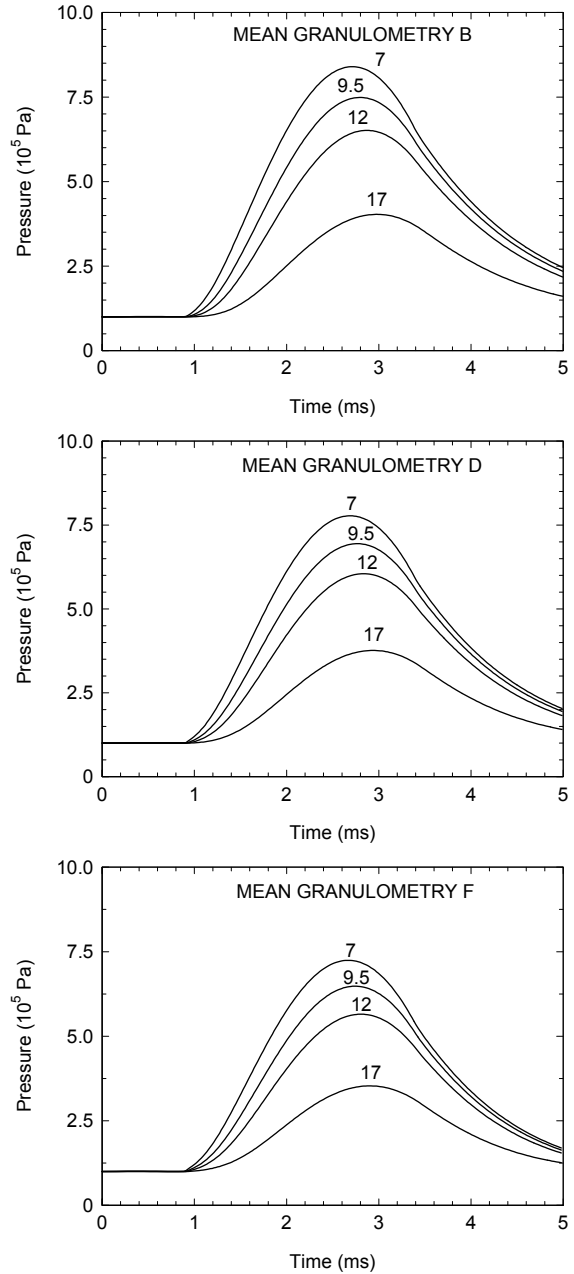

Fig. 8: Evolution of the fluid pressure versus time for the three mean granulometry values symbolized B, D, F. The numbers represent the position in the fuse domain (in mm).

Table 4. Maximum pressure observed for the three granulometries at various positions (d) in the fuse domain.

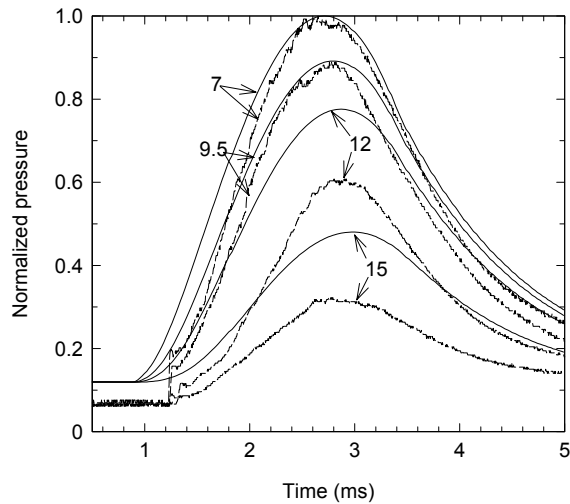| Granulometry	d (mm)			
	7	9.5	12	17
B	$8.4\ 10^5$	$7.5\ 10^5$	$6.5\ 10^5$	$4.0\ 10^5$
D	$7.8\ 10^5$	$6.9\ 10^5$	$6.1\ 10^5$	$3.8\ 10^5$
F	$7.2\ 10^5$	$6.5\ 10^5$	$5.7\ 10^5$	$3.5\ 10^5$

Fig. 9: Evolution of the normalized pressures versus time for the granulometry B. The numbers represent the position in the fuse domain (in mm). The full curves correspond to the simulation, the dash curves correspond to the experiment.
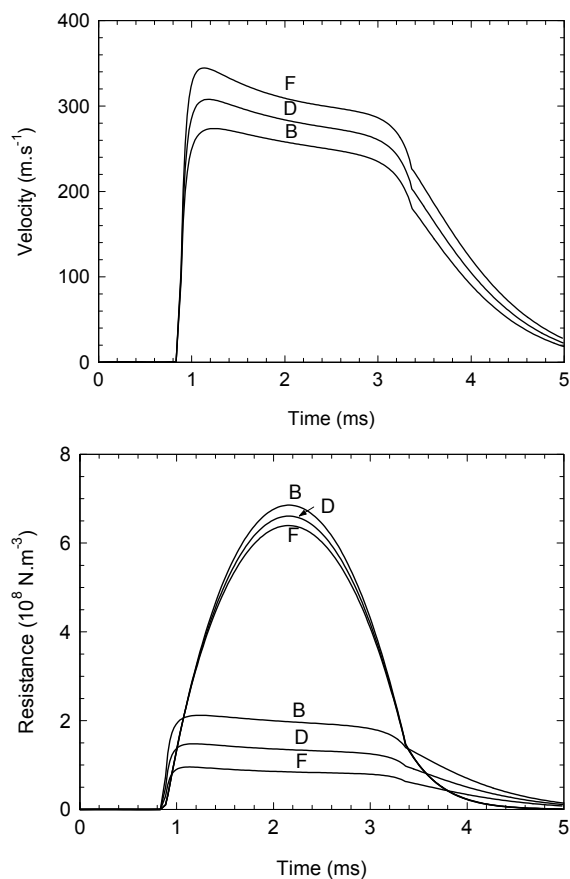

Fig.10: Evolution of the velocity and friction forces versus time for the three mean granulometry at the plasma periphery.

4. Conclusion

Due to the difficulty to access to the plasma pressure by a direct measurement, we have observed the pressure generated by the sand grains. The measurements are compared with a modeling based on the mechanical interaction between the fluid and the sand grains.

The two types of results are similar in so far as the studied area in the filler is not far from the plasma. For further areas, the modeling and the measurement show specific limitations. Especially, in the modeling, we attempt to consider the influence of the vapour recondensation, which should imply smaller pressures. At the present time, such calculations are helpful to test the influence of various morphometric property values on the H.B.C. fuse working.

Acknowledgements

References

[1] Saquib M.A., Stokes A.D., "Characteristics of fuse arcing in different fillers". *ICEFA* Turin 1999, p. 275.

[2] Sei-Hyun L., In-Sung K., Sang-Ok H., "The test method to acquire the optimal parameter for CL-fuse". *ICEFA* Turin 1999, p.265.

[3] Bussière W., "Estimation of the burn-back rate in high breaking capacity fuses using fast imagery", J. Phys. D: Appl.Phys., 34, pp 1007-1016, 2001.

[4] Bussière W., "Influence of sand granulometry on electrical characteristics, temperature and electron density during high-voltage fuse arc extinction", J. Phys. D: Appl.Phys., 34, pp 925-935, 2001.

[5] Saquib M.A., Stokes A.D., Seebacher P.J., "Pressure inside the arc channel of a high-voltage fuse". *ICEFA* Turin 1999, p.83.

[6] Rochette D., Clain S., "Numerical simulation of Darcy and Forchheimer force distribution in a H.B.C. fuse", Transport in Porous Media, 53, pp. 25-37, 2003.

[7] Rochette D, "Modélisation et simulation de la décharge d'arc electrique dans un fusible moyenne tension", Ph.D Thesis (in french), Blaise Pascal University.

[8] Jiang P.X., Ren Z.P. : Numerical investigation of forced convection heat transfer in porous media using a thermal non-equilibrium model,

International Journal of Heat and Fluid Flow, 22, 102-110, 2001.

[9] Toro E.F.: Riemann Solvers and Numerical Methods for Fluid Dynamics, Springer-Verlag, Berlin.

[10] RoHSENOW W.M., Hartnett J.P., Cho Y.I.: Handbook of Heat Transfer, McGraw-Hill Hanbooks, New York.

[11] Touzani R. : Object Finit Element Library Copyright © 1998-2001.